Experimental Section

Surface Characterization

The morphology and chemical composition of the electrodes used in this study have been analyzed by powerful complementary characterization techniques. Surface morphology has been examined with a Scanning Electron Microscope (SEM, Zeiss Supra 40, Oberkochen, Germany) equipped with a high-resolution cathode (Schottky field emitter), an Everhart-Thornley secondary electron (SE) detector and an InLens SE detector. Chemical composition of the bulk of the sample material (up to 1 µm) was investigated by Energy-Dispersive X-Ray Spectroscopy (EDS). EDS is a method integrated to the most SEMs and is well suited for quick qualitative elemental analysis with a spatial resolution from the micrometer range down to 10 nm [1]. EDS spectra were measured with an SDD (silicon drift detector) EDS system (Thermo Fisher Scientific, Waltham, MA, USA) with a nominal detector area of 100 mm^2 [2] . Furthermore, the EDS analysis has been supplemented by the highly elemental sensitive technique (ppm range) Time-of-Flight Secondary Ion Mass Spectrometry (ToF-SIMS, TOF.SIMS IV, IONTOF GmbH, Münster, Germany). The lateral resolution attained by this technique is in nano scale under optimal conditions (~100 nm)[3]. These two analytical techniques have enabled a reliable complementary chemical imaging of the surface of the electrodes.

The working electrodes (WE) of the following samples were analyzed by ToF-SIMS: unused carbon screen-printed electrode (C), carbon screen-printed electrode after use at pH 4 and cyclic voltammetry with 500 µM TMB (C pH 4) and unused carbon electrode spin-coated with TMB (C TMB). The TMB control experiment was prepared as follows: TMB (40 mM) was dissolved in DMA. A 20 µL drop was spin-coated onto an unused electrode, before being dried in a vacuum desiccator and stored in the loading chamber of the ToF-SIMS overnight at 10^{-6} mbar. Samples were analyzed in the ToF-SIMS as described below. In each case, only the working electrode (WE) was analyzed. Spectra were taken in several different locations (Loc) on the WE, however effort was made to avoid the area, which was likely to contain adhesive contamination, as shown in Figure S6 a. For principal component analysis (PCA), at least 5 spectra are preferable for analysis.

Spectra were measured in both positive and negative mode in several different locations on the working electrode, on an IONTOF ToF-SIMS IV instrument in spectrometry mode (HCBU) with a 25 kV Bi_3^+ primary ion beam in static SIMS mode with a maximum dose density of 10^{12} ions cm^{-2}. A field of view of 100 x 100 μm^2 was scanned in sawtooth mode with 125 x 125 pixels. Charge compensation was applied. Spectra were analyzed using SurfaceLab 7, using the same calibration peaks and peak list for all spectra. PCA was performed using Solo+MIA software from Eigenvector Research, Inc, and using the following pre-processing steps performed manually in Excel: Normalization to total area, divided by the square root of the standard deviation, and mean centered.

Raman spectroscopy

Raman spectra were measured with a LabRam HR 800 instrument (Horiba Jobin Yvon) coupled to a BX41 microscope (Olympus) as reported by Schmid and Dariz[4]. A 50x/NA = 0.55 long working distance objective lens was employed for excitation and collection of the scattered light. The system is equipped with a diode-pumped solid-state (DPSS) laser (532 nm wavelength and 300 mm^{-1} grating) offering a resolution of the spectra that were acquired with a Peltier cooled (-60°C operating temperature) charge-coupled device (CCD) camera (Syncerity CCD, Horiba Jobin Yvon)

of approximately 3.4 cm^{-1} per CCD pixel at 1000 cm^{-1} Raman shift, 3.2 cm^{-1} at 1500 cm^{-1} and 2.6 cm^{-1} at 3000 cm^{-1}. The entrance slit of the spectrometer was 100 µm wide and the confocal pinhole was in the fully open position (1000 µm). Before the measurements with the electrodes were performed, the laser was allowed to stabilize for 1 h and the spectrometer was recalibrated against the most prominent Raman band of silicon at 520.7 cm^{-1}.

After cyclic voltammetry with TMB at carbon and gold screen-printed electrodes has been performed at pH 1 and pH 4 the electrodes were rinsed with ultrapure water and the surfaces were analyzed by Raman spectroscopy to study if TMB remains at the electrode. To produce a reference spectrum of oxidized TMB precipitates occurring after cyclic voltammetry with TMB at pH 4 one electrode of each type was prepared without removing the TMB precipitates by rinsing with ultrapure water. The Raman spectra were measured at marked spots in the light micrographs (see Figures S14 and S15) with a laser power of 4 mW (full power attenuated to 10% while using a neutral density filter). The laser spot diameter under the chosen conditions is approximately 1 µm, while the depth resolution in transparent samples with open confocal pinhole is estimated to amount to approx. 40 µm[4]. In the strongly reflective gold as well as in the highly absorbing and scattering carbon electrode materials, the depth resolution is limited by the optical penetration depth.

MALDI-TOF/MS

To determine the degree of labelling of the HRP tracer with OTA, MALDI-TOF/MS (Autoflex III, Bruker Daltonics, Bremen, Germany) was applied. All experiments were performed with a nitrogen laser at an acceleration voltage of 20 kV. 10 µL of HRP and the OTA-HRP tracer (1.8 mg mL^{-1}) were desalted with a Zeba™ Micro Desalt Spin Column which was centrifuged at 10,000 rpm for 90 s. The samples were eluted with 10 µL of Milli-Q water and mixed with 50 µL of dihydroxyacetone phosphate (DHAP) matrix. 375 µL of DHAP matrix solution (20 mg mL^{-1} in ethanol) were mixed with 125 µL of diammonium citrate solution (18 mg mL^{-1} in H_2O). Finally, a mixture of 2 µL of the matrix, 2 µL of the sample and 2 µL of 2% trifluoroacetic acid was applied to the target and dried before the MALDI-TOF/MS measurement was performed.

Results and Discussion

SEM and EDS analysis

An important issue before taking SEM images and performing EDS analysis was sample preparation. Nonconducting samples (surface) tend to charge when excited by the electron beam, especially in secondary electron (SE) imaging mode. This causes image distortion. To eliminate electric charge, a piece of aluminum adhesive tape was gently attached to a small portion of the working electrode's surface. The other end of the tape was connected to the sample holder. This provided a path for the "trapped" electrons to flow to ground during SEM analysis [5].

The SEM images of the gold electrodes are shown in Figure S1. Figures S1a, b, and c reveal clear evidence of pores within the material of the working electrode for unused and both used electrodes. It was observed that the porous structure is present over the entire surface of the working electrode.

This porosity is formed during the screen-printing of the electrodes. SEM images reveal that the platinum counter electrodes of all gold screen-printed electrodes show a sponge-like structure and the reference electrodes have relatively larger pores compared to the working electrode. The difference in the surface morphology between working electrode, counter electrode and reference electrode is expectable since they are made of different materials (Au, Pt, Ag, respectively). However, no significant morphological difference was observed between all three gold electrode samples: unused electrode, used electrode at pH 1 and used electrode at pH 4 (after cyclic voltammetry with 500 µM TMB has been performed).

The surface morphology of working electrode and counter electrode in case of the set of carbon electrodes is different than that of the gold electrodes, see Figure S2. The surface morphology of the reference electrode in the case of the carbon electrodes is similar to that of gold electrodes. The common feature of carbon and gold electrodes is that they all have a porous structure on the surface of all types of electrodes. Similar to the gold electrodes, no significant morphological difference was observed between all three carbon electrode samples.

The chemical formula of TMB is $C_{16}H_{20}N_2$, thus, it was aimed to identify TMB by detecting the presence of nitrogen (N) via EDS analysis. EDS analysis was performed only on the surface of the working electrode of an unused screen-printed carbon electrode and a used carbon electrode at pH 4. Three different locations on the surface of the working electrode, as schematically depicted in Figure S3b, were selected to check for the qualitative evidence on nitrogen presence. The first location was an area at the center of the working electrode (Loc1), the second location was an area between center and border of the working electrode (Loc2), and the third location was an area which was near the border of the working electrode (Loc3). Two areas with a field of view (FOV) of 100 x 100 μm^2 at each location were analyzed (Figure S3c). This approach yields detailed information on the homogeneity of the elemental composition of the working electrode.

Figure S4 presents SEM images of three different locations of the working electrodes where EDS analysis was performed. Regardless of whether the electrode is used or unused, a porous structure was clearly visible overall on the surface of the working electrode. Further extensive analysis is necessary to precisely quantify the size and distribution of these pores, however, this is out of the scope of this work. For both electrodes, no significant morphological difference was observed in the SEM images.

The EDS spectra for determining the elemental composition of the electrodes is presented in Figure S5. The results of EDS measurements carried out with unused carbon electrode and used carbon electrode at pH 4 are shown in Figures S5 a and b, respectively. All EDS spectra presented here were normalized to the highest detected O K X-ray peak intensity for each sample. A very high C K peak intensity was detected for both samples since carbon is the major constituent element of the working electrode material itself. Although the samples should not contain any silicon (Si), a very low Si K signal was detected in both samples. Sulfur and chlorine were also detected because the sample surface could be contaminated during pre- or post-treatment. However, no nitrogen was detected in both unused and used electrode, which suggests that no significant fraction of TMB remained on the surface of the samples. It should be noted that the limit of detection for nitrogen by EDS is relatively poor (~1 wt-%) [6].

These results can be explained in two ways: either the nitrogen concentration level in the µm-bulk of the samples is lower than the detection limit of EDS system or nitrogen remained in a very thin

(nm) layer only on the surface and EDS cannot sense it. Therefore, further chemical analysis was conducted by ToF-SIMS which investigates the outermost sample surface and provides chemical analysis of molecular ionic fragments with high sensitivity down to ppm levels, see later. Based on the information delivered by EDS, both electrodes can be considered as homogeneous in terms of elemental composition. Additionally, both electrodes are very similar in elemental composition as it is suggested by Figure S5c.

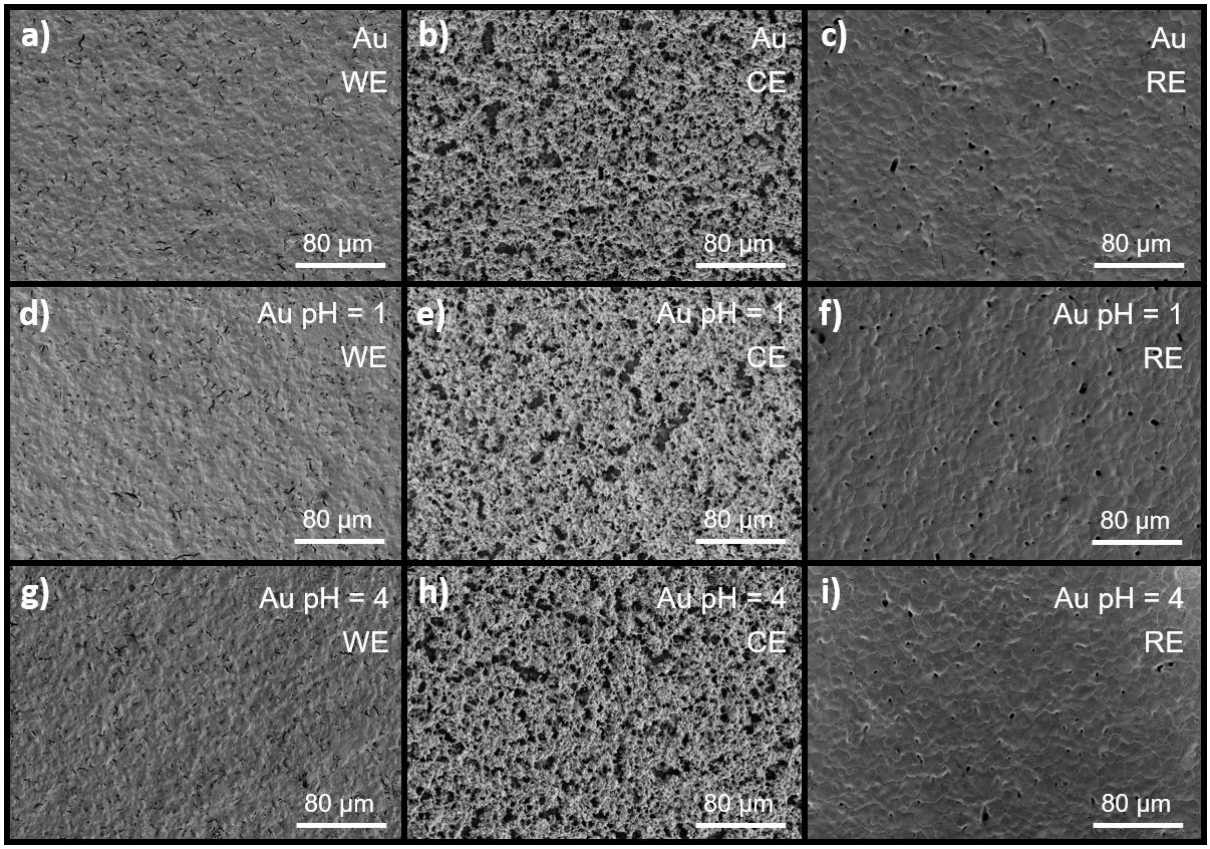

Figure S1 SEM images of the surface of an unused screen-printed gold electrode: **a)** WE, **b)** CE, **c)** RE, of a used screen-printed gold electrode at pH 1: **d)** WE, **e)** CE, **f)** RE, of a used screen-printed gold electrode at pH 4: **g)** WE, **h)** CE, **i)** RE. All SEM images were taken at 5 kV. (Au: gold, WE: working electrode made of gold, CE: counter electrode made of platinum, RE: reference electrode made of silver, SEM images d-i were taken after cyclic voltammetry with 500 µM TMB has been performed and after rinsing the electrodes with ultrapure water).

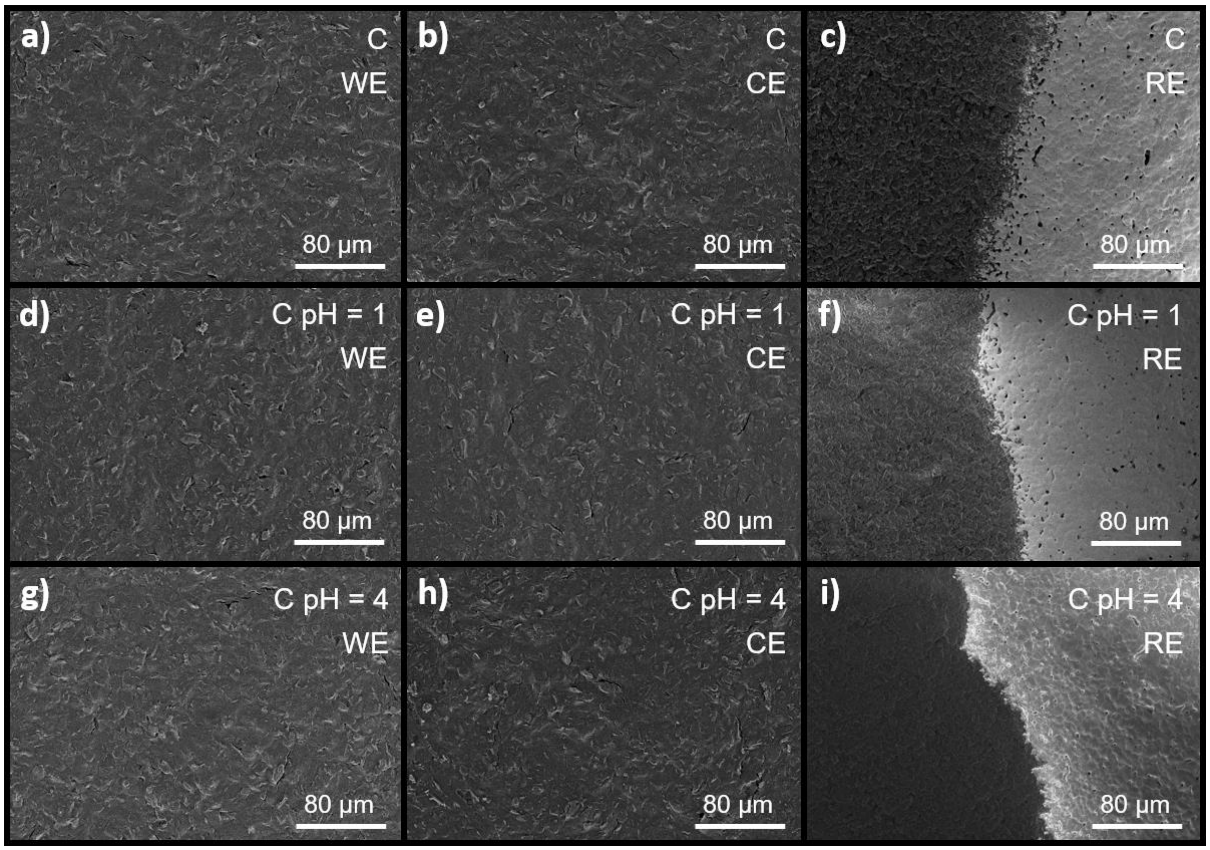

Figure S2 SEM images of the surface of an unused screen-printed carbon electrode: **a)** WE, **b)** CE, **c)** RE (right side of the image), of a used screen-printed carbon electrode at pH 1: **d)** WE, **e)** CE, **f)** RE (right side of the image), of a used screen-printed carbon electrode at pH 4: **g)** WE, **h)** CE, **i)** RE (right side of the image). All SEM images were taken at 5 kV. (C: carbon, WE: working electrode made of carbon, CE: counter electrode made of carbon, RE: reference electrode made of silver, SEM images d-i were taken after cyclic voltammetry with 500 µM TMB has been performed and after rinsing the electrodes with ultrapure water).

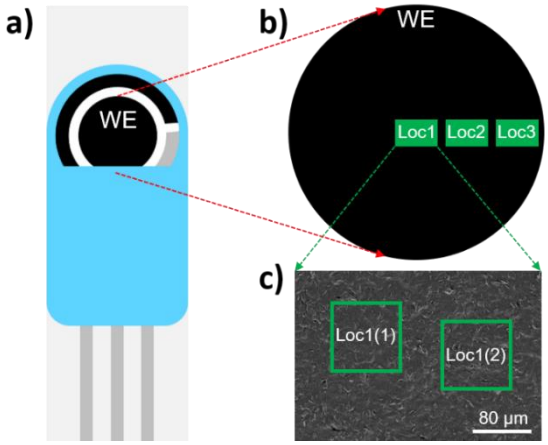

Figure S3 Schematic illustration of **a)** a screen-printed carbon electrode, **b)** selected 3 locations, and **c)** selected 2 fields (each 100 x 100 μm^2) in a location on the surface of the working electrode to perform EDS analysis. (WE: working electrode, Loc1 = location 1: center, Loc2 = location 2: between center and border, Loc3 = location 3: near border).

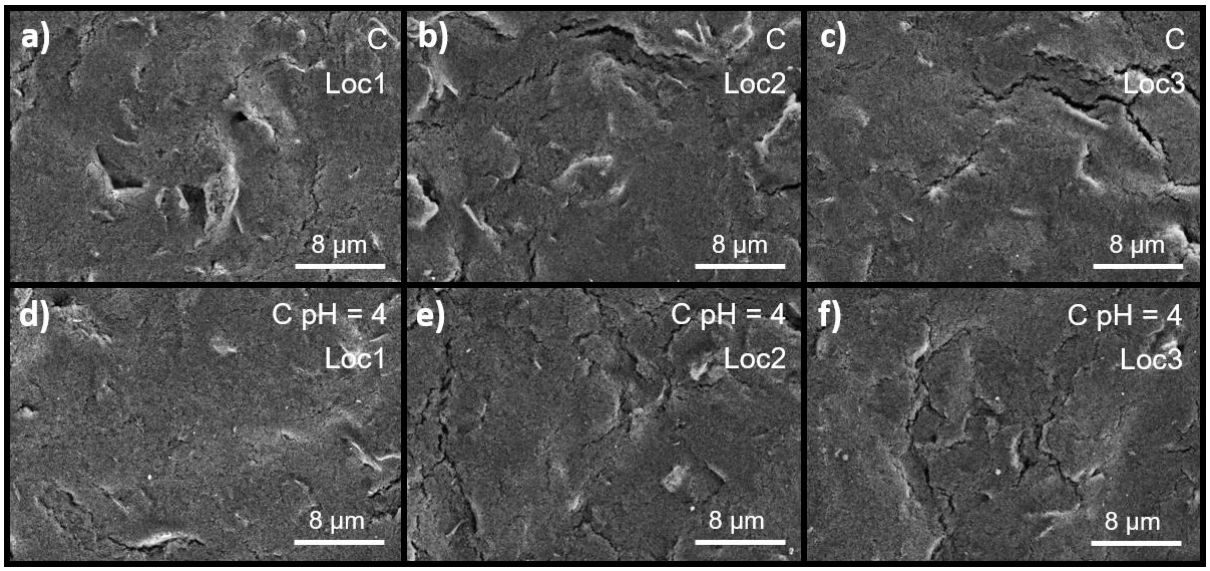

Figure S4 SEM images of the working electrode showing the locations where EDS analysis has been performed: **a)** center, **b)** between center and border, **c)** near border of the working electrode of an unused carbon electrode, **d)** center, **e)** between center and border, **f)** near border of the working electrode of a used screen-printed carbon electrode at pH 4. All SEM images were taken at 5 kV (C: carbon, Loc1 = location 1: center, Loc2 = location 2: between center and border, Loc3 = location 3: near border).

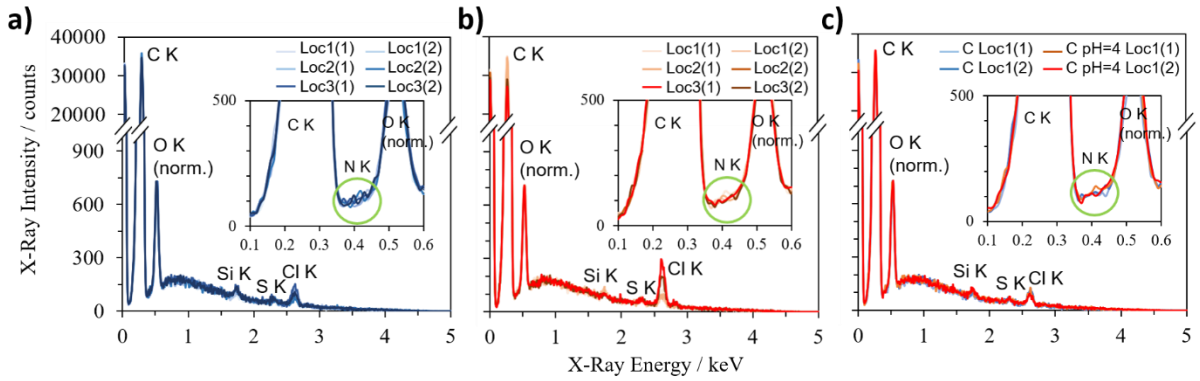

Figure S5 5 kV EDS analysis on the surface of working electrode of **a)** an unused carbon electrode, **b)** a used carbon electrode at pH = 4. **c)** shows comparison of unused and used carbon electrode at pH 4 for the center position. Selected 2 fields (each 100 x 100 µm^2) in a location to perform EDS analysis are indicated in the parenthesis. (C: carbon, Loc1 = location 1: center, Loc2 = location 2: between center and border, Loc3 = location 3: near border).

ToF-SIMS analysis

ToF-SIMS is a highly surface-sensitive analytical method which has been used for diverse applications including materials science[7], nanotechnology[8], biology [9] and cosmochemistry[10]. It involves the bombardment of a surface with an ion beam which causes molecular fragmentation

of the sample and ejection of a variety of species such as positive and negative ions, as well as electrons and neutral species. The positive or negative ions respectively are extracted using an electric field and analysed using a Time-of-Flight mass analyser which separates the extracted molecular and atomic ions according to their m/z (mass-to-charge) ratio. ToF-SIMS is therefore able to provide highly accurate m/z values and is able to separate different isotopes of species Although ToF-SIMS provides sensitivity in the ppb range, it can provide at most semi-quantitative analysis. ToF-SIMS provides information on the first 1-3 nm of the sample, and by limiting the ion flux the technique can be considered non-destructive. [11]

In this work, ToF-SIMS is used for the detection of peaks related to TMB, and the comparison of the unused electrode, used electrode and an electrode coated with TMB. Due to the complexity of ToF-SIMS spectra and the large number of peaks, spectra were analysed using PCA. PCA is a method of multivariate analysis in which the data are transformed to a new set of axes (the principal components) in order to maximise the variance of the data; this approach reduces the dimensionality of data sets and allows the results to be more easily analysed and grouped. [12] The results are plotted in Scores and Loadings plots which are to be analysed concurrently. The Scores plots represent the distance of each point representing one spectrum from the mean of all spectra and show the relationship or differences between the sample sets (i.e. are the sample sets similar to each other). The Loadings plots, on the other hand, are an analysis of the factors which most strongly affect PCA scores and show the relationship between variables, in this case ToF-SIMS peaks. Loosely described, the graphs answer the questions: are the samples different from each other, and which peaks are the cause of the difference? The different PCs (principal components) describe the 1st, 2nd, 3rd (and so on) sources of difference in the form of PC1, PC2, PC3, etc.

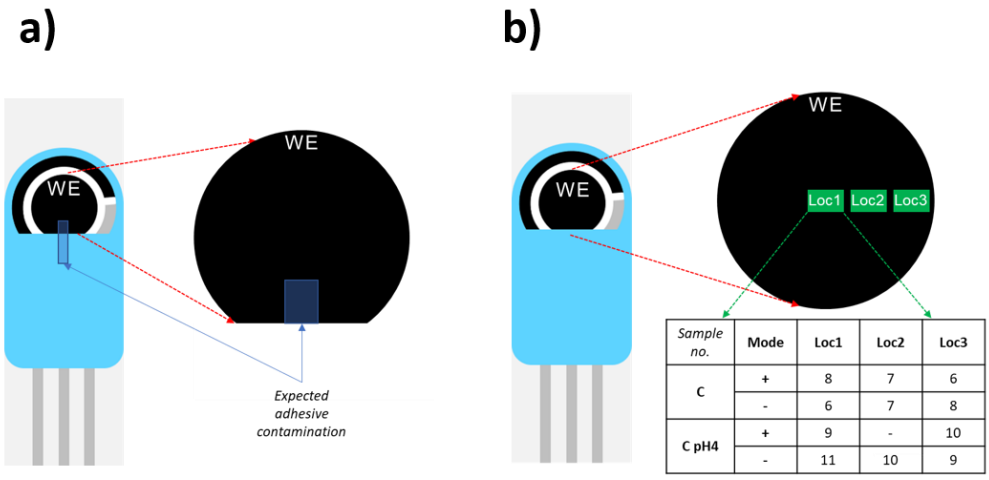

Sample no.	Mode	Loc1	Loc2	Loc3
C	+	8	7	6
	-	6	7	8
C pH4	+	9	-	10
	-	11	10	9

Figure S6 a) Electrode showing the working electrode and expected location of adhesive contamination which was avoided for analysis. b) Approximate locations of EDS measurements and table comparing the corresponding ToF-SIMS samples, for positive and negative mode. In the negative mode these were samples no. 6-8 and 9-11 respectively, and in the positive mode samples nr. 6-8 and 9-10 respectively.

Negative mode: H^- and Cl^- ions were excluded from analysis since strong ionisation in the negative mode, which can cause peak saturation and lead to biases in the analysis. The aim of the analysis was to determine if the two used electrodes could be differentiated from each other, and if they could be differentiated from the sample which was spin-coated with TMB. If the C-TMB sample showed a similar mass spectrum to the C pH4 electrode, it could be concluded that TMB was

present on the electrode. Due to technical difficulties it was not possible to measure exactly the same areas which were analysed via SEM/EDS.

Analysis in the negative mode showed that in PC1 (the major cause of difference between all the samples) the C TMB samples showed a clear difference from the C and C pH4 electrodes. The samples with the high scores, in this case C TMB, correspond to the peaks with the higher loadings plots; in this case CN-, C2- and C4- peaks, which are consistent with TMB fragments. These samples also have a high content of Bromine as seen in the Br- and 81Br- peaks; the source of this contamination is unclear but may come from less than ultrapure-quality water. The C and C pH4 samples, on the other hand, correspond to peaks containing C, H, F, S, N, and particularly P species. This suggests that traces of TMB cannot be used to differentiate the C from the C pH4 electrodes as hoped. The large variation in PC1 between the different regions of interest on the C electrode indicates some kind of contamination on the electrode; detection of contamination is common in the first principal component and is a useful source of information. [12b] In this case, the most likely scenario is that one or more regions of interest measured contained adhesive residues.

PC2 describes the second-greatest source of variation within the samples. In this case, the large difference between the different C electrode measurements in the first measurement round. This is attributed to various hydrocarbons containing O, S, P and N. Due to the large variance between 3 regions of interest, and the relatively small difference between all other samples, we attribute this to measurement of contaminated areas of the working electrode, most probably contaminated with adhesive.

Due to the large amount of variation within the C and C pH4 samples as shown in Figure S9, it is not possible to differentiate the electrodes from each other. However, by graphing PC1 and PC3 together, the three different samples can be successfully differentiated from each other, which is one purpose of PCA (this is unsuccessful with other combinations of principal components).

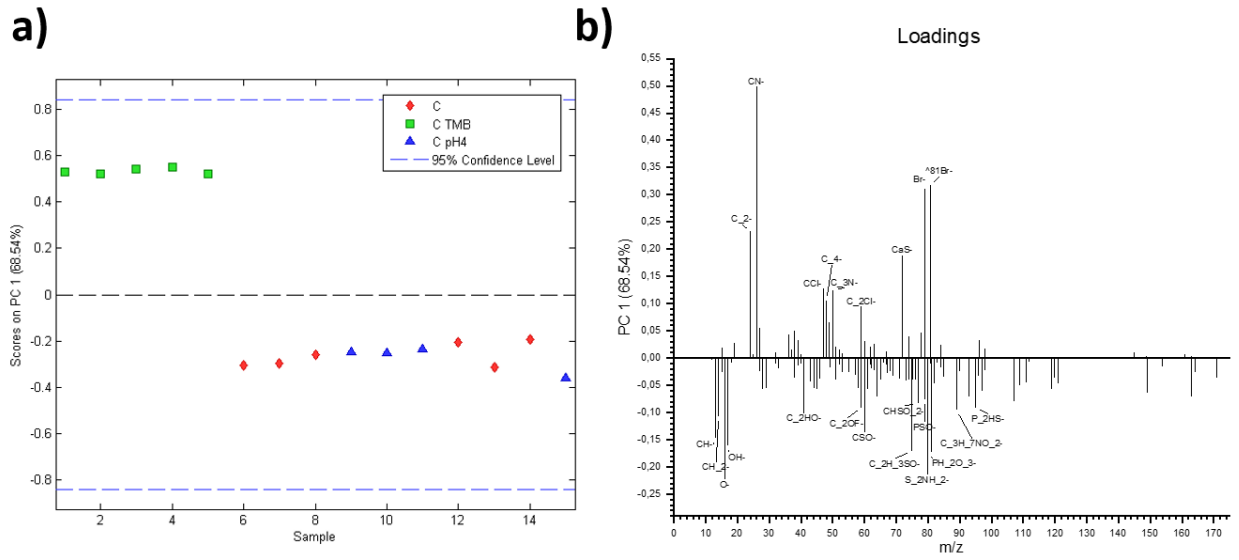

Figure S7 a) Scores and **b)** loadings plots for PC1 in the negative mode. For legibility only the high-scoring peaks in the loadings plot are labelled.

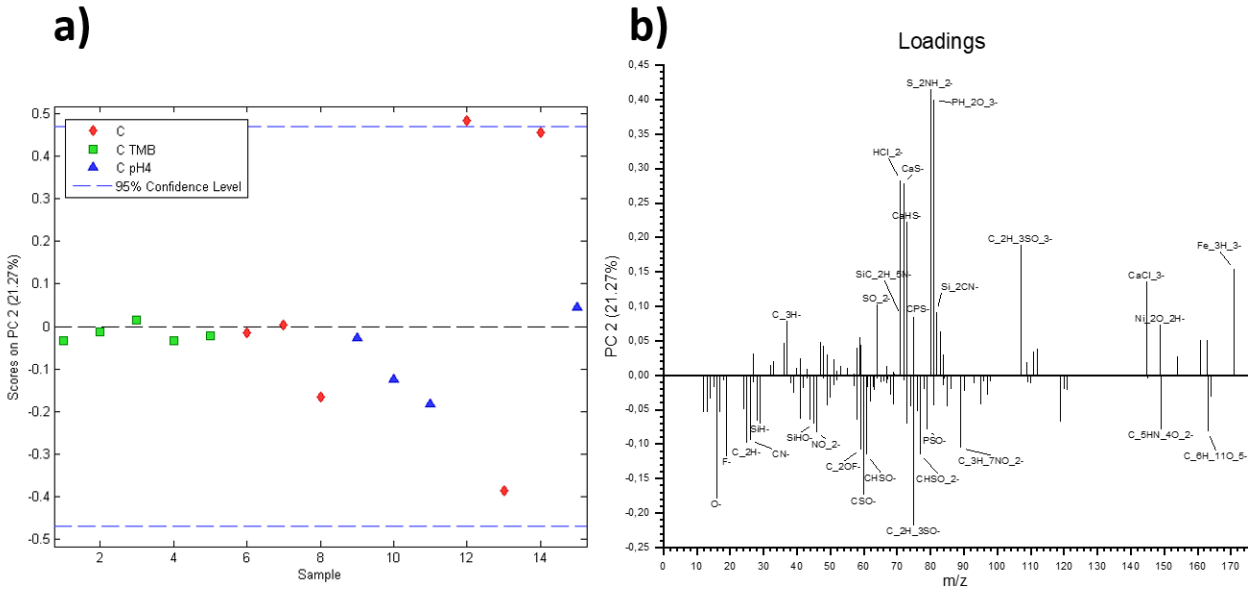

Figure S8 a) Scores and **b)** loadings plots for PC2 in the negative mode. For legibility only the high-scoring peaks in the loadings plot are labelled.

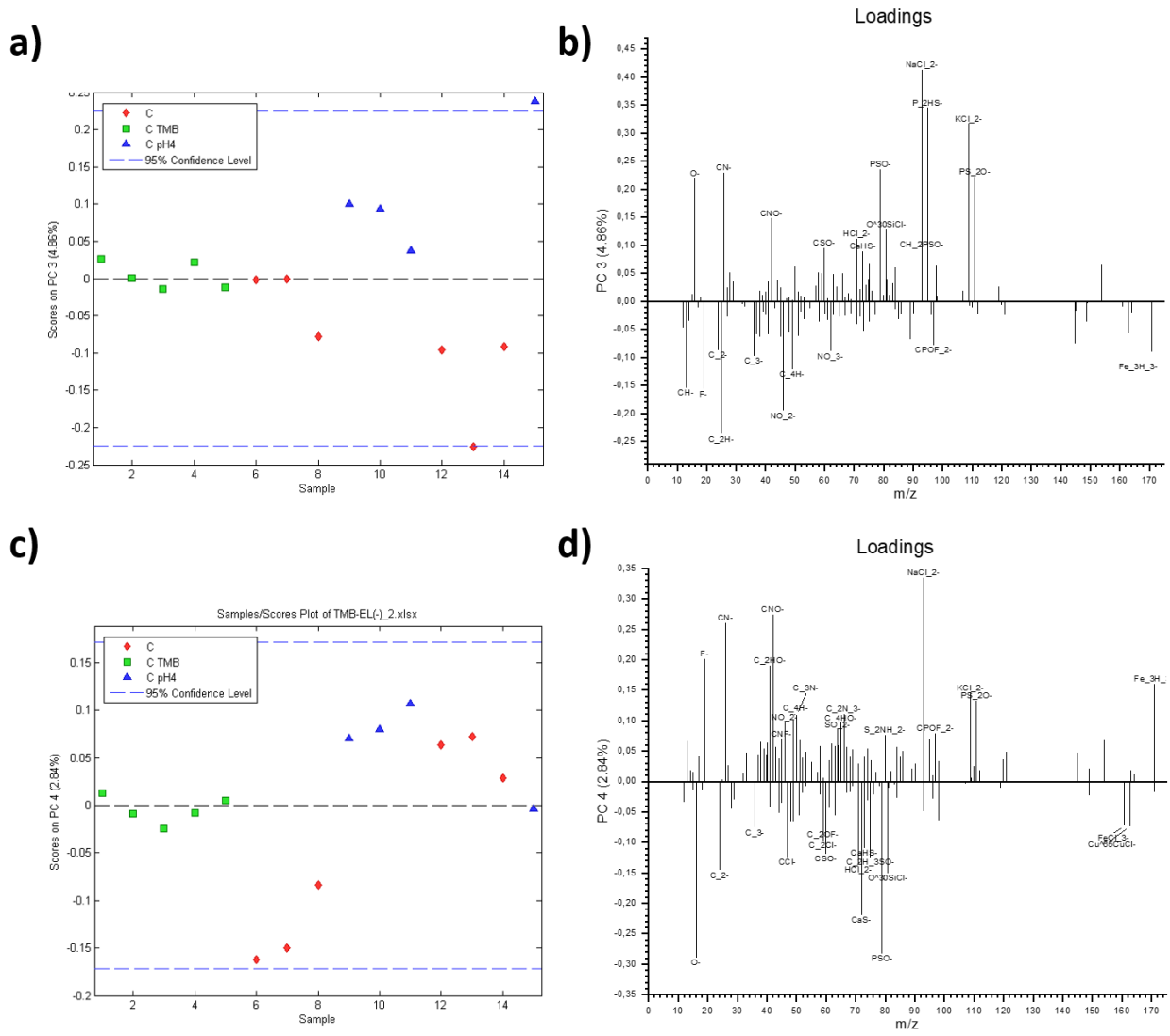

Figure S9 a) Scores and **b)** loadings plots for PC3 and scores **c)** and loadings **d)** plots for PC4, showing the large variation within samples compared to between samples.

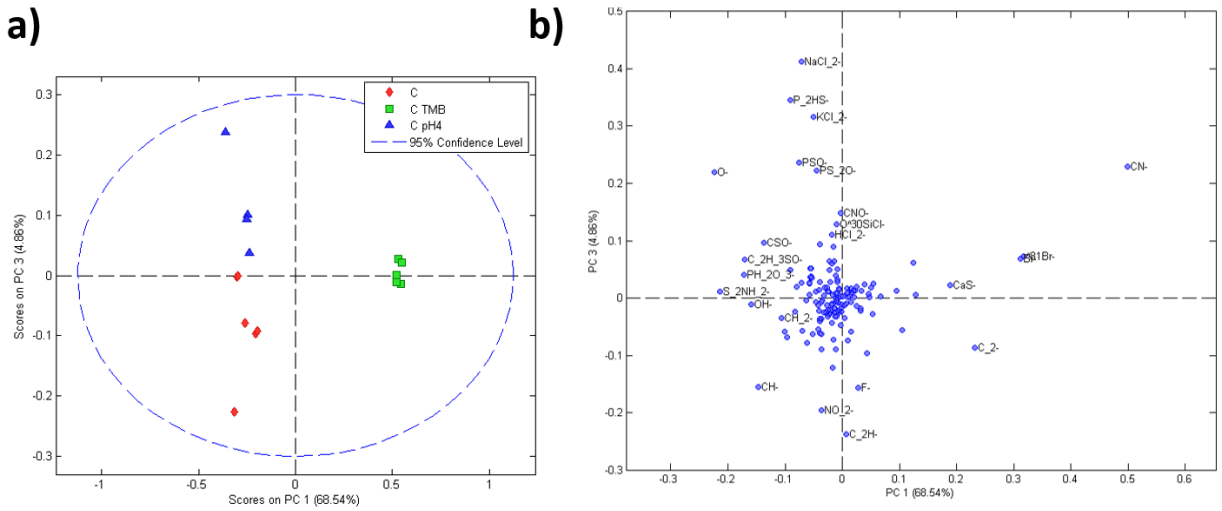

Figure S10 a) Scores and **b)** loadings plots for PC1 and PC3 combined, demonstrating an ability to differentiate the samples from each other.

Positive mode: Because some species ionise much more readily than others, and some species much more readily form positive rather than negative ions (and vice versa), it is important to measure both positive and negative ions emitted from the sample after bombardment with the primary ion beam. Due to the difference in species ionised, both the mass spectrum and PCA may yield dramatically different results, including the number of principal components in the model. For the positive mode, a model was chosen based on only 2 principal components, since they explained a sufficient proportion of the variance within the sample.

The scores plot for PC1 shows that the largest source of variation between the sample groups is between C TMB and the C and C pH4 samples, respectively. The cause of this variation is peaks relating to CxHy and CxHyN, which correspond to the TMB spin-coated on the electrode. The C pH4 peaks which were suspected to contain TMB show a clear difference to the C TMB samples; this would indicate that the presence of TMB is not the source of the different performance between the C pH4 and the C electrodes.

Both the C and C pH4 electrodes show higher loadings from peaks related to inorganic species such as Na, K, Al and Si, as well as some hydrocarbon peaks likely resulting from adventitious contamination during sample handling. Particularly noteworthy were the several peaks containing SiCxHy, with or without N or O. Si-based contamination may occur from traces of adhesive left on the electrode; siloxanes are commonly used as release coatings on adhesive liners. Na and K species are possibly residues from water with less than ultrapure quality.

All three samples, however, can be clearly differentiated in the graph combining PC1 and PC3 (see Figure S10); it is noteworthy here that the C and C pH4 samples can be very clearly differentiated. C pH4 contains a number of inorganic peaks including Na, K, K2F, K2Cl and Na2Cl, among others. The large number of CxHy or CyHyN peaks with a PC3 loading close to zero is consistent with the C TMB sample, while the C electrode contains stronger peaks with the CxHySi or CxHyAl formula. The scores plot in Figure S13 shows that the three samples can in this case be clearly

differentiated when the first two principal components are plotted together, along with the prominent peaks in their positive ToF-SIMS spectra, summarised in Table 1:

Table 1		
Sample	Prominent species in positive spectra	Possible source
C	CxHy, CxHySi, CxHyAl	Adventitious hydrocarbons, unknown sources, Si and Al from manufacture
C pH4	Na, K, K_2F, K_2Cl, Ca_2F	Inorganic contamination from water or other chemicals
C TMB	CxHy, CxHyN	TMB and adventitious surface hydrocarbons

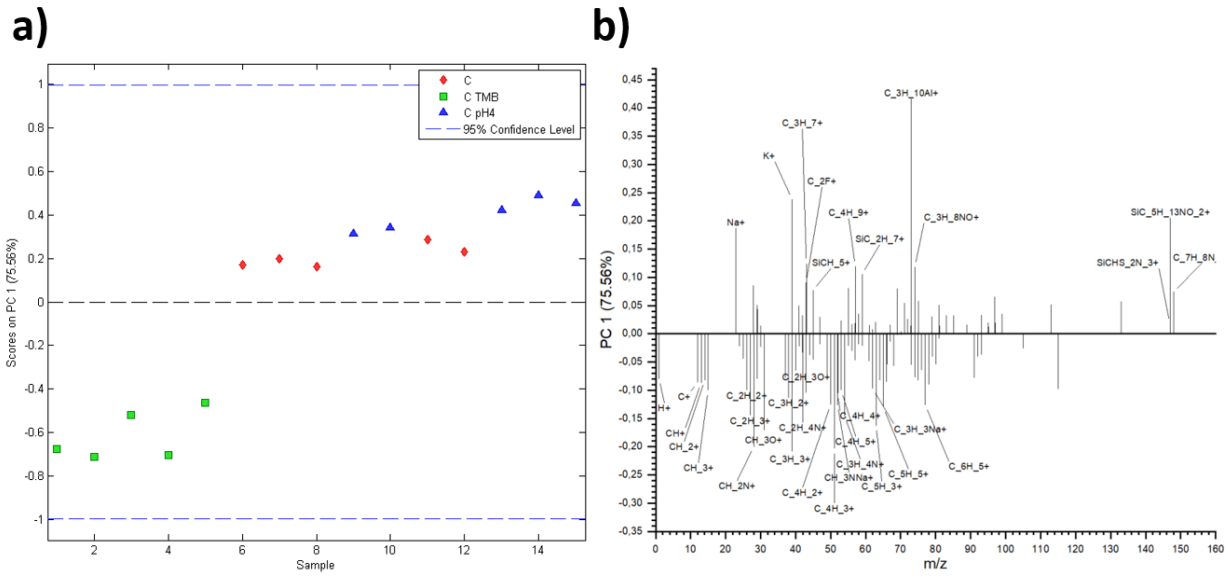

Figure S11 a) Scores and **b)** loadings plots for PC1 for positive ions.

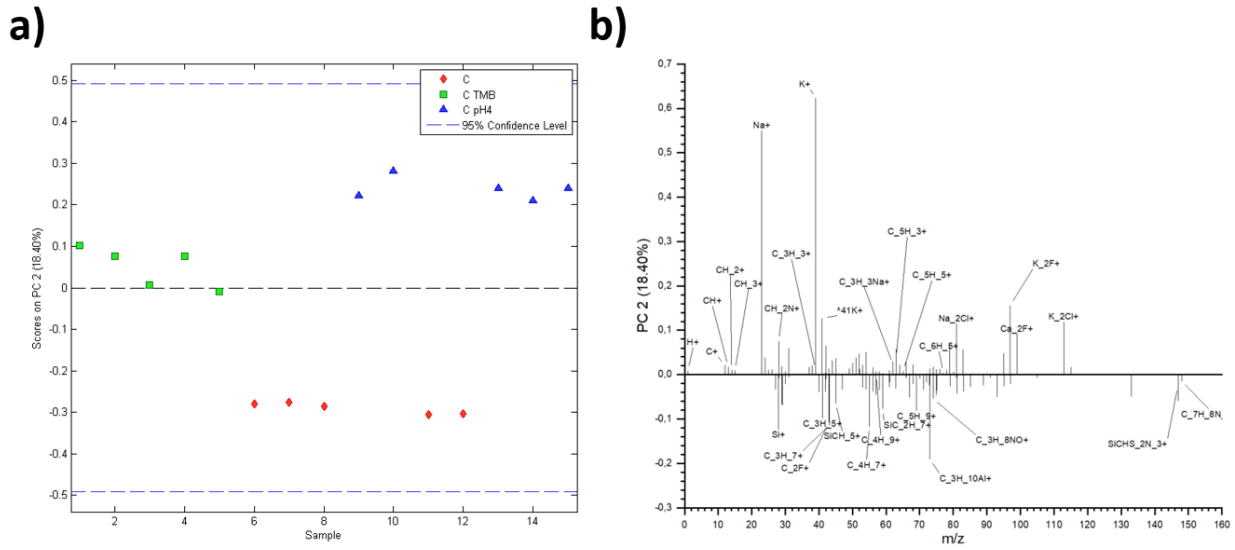

Figure S12 a) Scores and **b)** loadings plots for PC2 for positive ions.

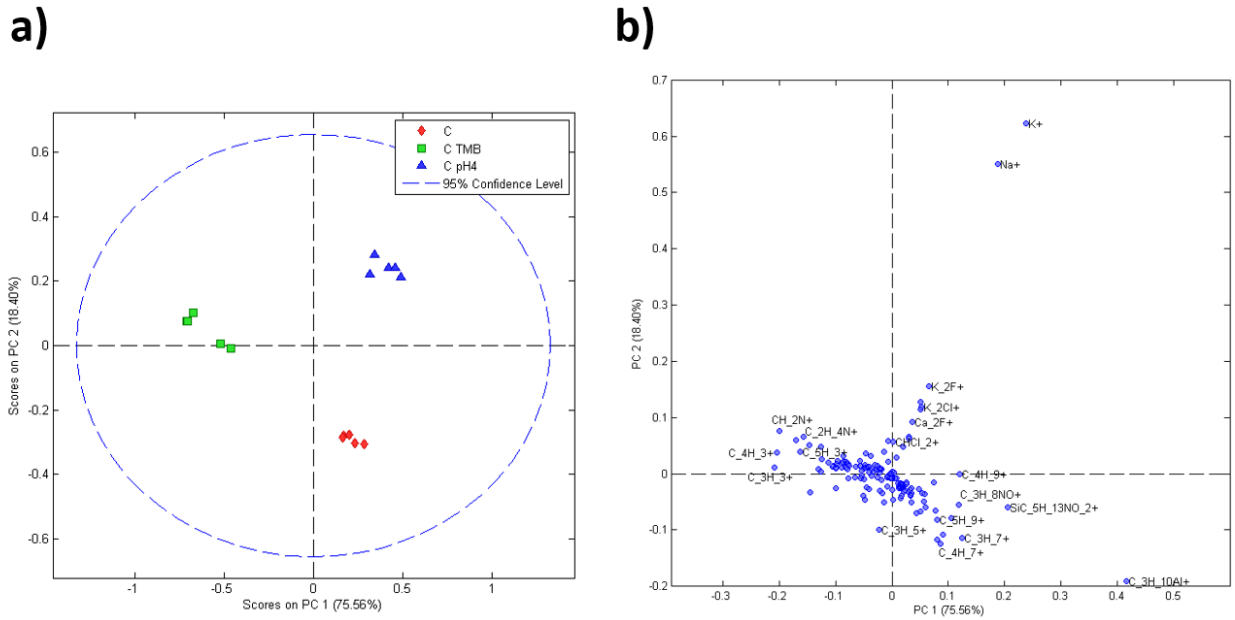

Figure S13 a) Scores and **b)** loadings plots for PC1 and PC2 for positive ions, showing a clear differentiation between all three samples.

The spectra in the negative mode (analyzed excluding H- and Cl- as they ionize very strongly in the negative mode and can distort the PCA analysis) show a greater variation within samples than between samples, particularly for the C and C pH 4 samples (the C TMB samples show relatively consistent results over the different locations analyzed). This would indicate some contamination within different measurements, particularly as the C and C pH4 samples were each measured on two separate occasions. However, this is inconsistent with the analysis of spectra in the positive mode in which the samples can be clearly differentiated according to their pre-treatment; if contamination were the largest source of difference between all the locations measured, this should also appear in the positive mode. The differences in results across one electrode may then be due

to local inhomogeneities on the electrode surface, combined with different choice of locations for measurement in different modes, and the different ionization probability of various species in positive or negative modes, respectively. However, the results from analysis in the positive mode can in any case clearly differentiate between the three electrodes with relatively small variation within electrodes. From this we can conclude that there is not a significant amount of TMB present at the surface of the C pH4 electrode, which can be clearly separated from both the C TMB and the C electrode with their corresponding characteristic species as seen in Figure S13 and Table 1.

Raman microspectroscopy

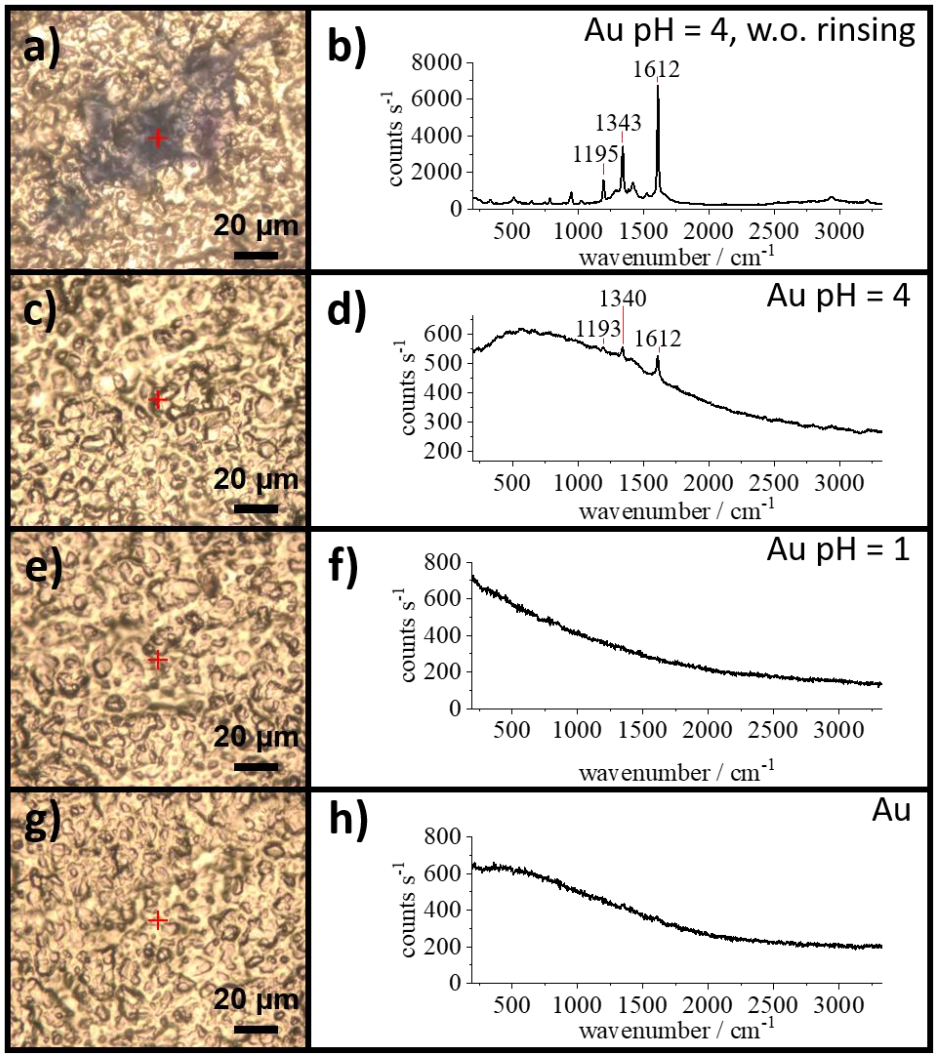

Figure S14 Light microscopic images and corresponding Raman spectra of screen-printed gold electrodes. **a)** and **b)** were obtained after cyclic voltammetry in 500 µM TMB at pH 4 in 220 mM sodium citrate buffer with 100 mM KCl was performed without removing visible TMB precipitates by ultrapure water. a) shows a blue TMB precipitate on the gold surface of the working electrode. **c)** and **d)** were obtained after cyclic voltammetry in 500 µM TMB pH 4 in 220 mM sodium citrate buffer was performed and subsequent rinsing of the electrode with ultrapure water. **e)** and **f)** show the results after cyclic voltammetry in 500 µM TMB at pH 1 in 150 mM sodium citrate buffer with 300 mM H_2SO_4 and 100 mM KCl was performed and subsequent rinsing of the electrode with ultrapure water. **g)** and **h)** were obtained from the bare gold electrode surface as reference. All spectra were measured at the red marked spots in the light micrographs with 532 nm excitation wavelength, a laser power of 4 mW (full power attenuated to 10% while using a neutral density filter) and a laser spot diameter of approximately 1 µm. As different acquisition times were applied (b, f, and h: two averaged acquisitions of 5 s each; d: 4 acquisitions of 30 s each) to avoid saturation of the detector and to ensure detection of the small amounts of TMB after rinsing, the intensity axes are expressed in counts per seconds to enable best comparability.

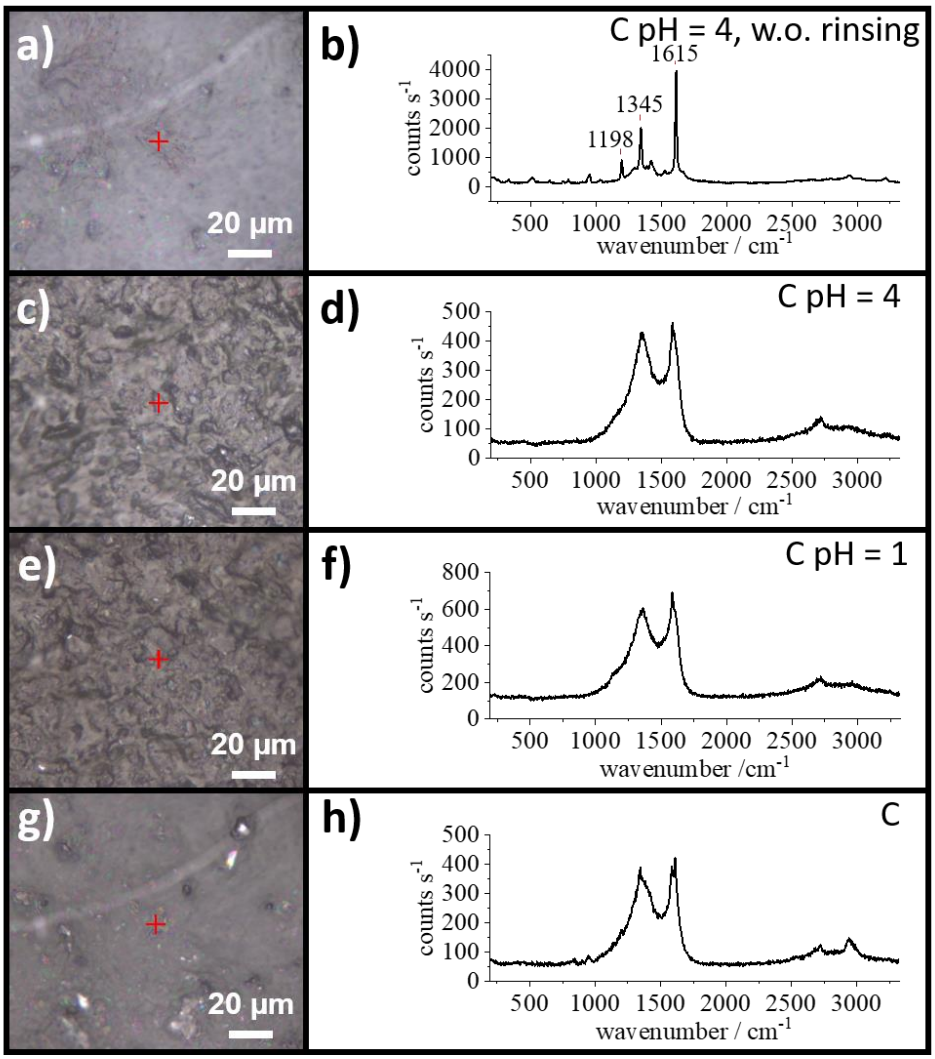

Figure S15 Light microscopic images and corresponding Raman spectra of screen-printed carbon electrodes. **a)** and **b)** were obtained after cyclic voltammetry in 500 µM TMB at pH 4 in 220 mM sodium citrate buffer with 100 mM KCl was performed without removing visible TMB precipitates by ultrapure water. **c)** and **d)** were obtained after cyclic voltammetry in 500 µM TMB pH 4 in 220 mM sodium citrate buffer was performed and subsequent rinsing of the electrode with ultrapure water. **e)** and **f)** show the results after cyclic voltammetry in 500 µM TMB at pH 1 in 150 mM sodium citrate buffer with 300 mM H_2SO_4 and 100 mM KCl was performed and subsequent rinsing of the electrode with ultrapure water. **g)** and **h)** were obtained from the bare carbon electrode surface as reference. All spectra were measured at the red marked spots in the light micrographs with 532 nm excitation wavelength, a laser power of 4 mW (full power attenuated to 10% while using a neutral density filter) and a laser spot diameter of approximately 1 µm.

Cyclic Voltammetry

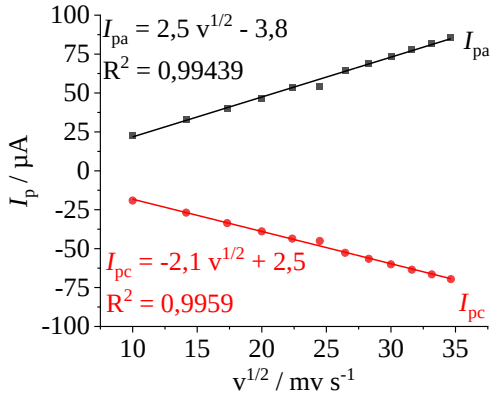

Figure S16 Peak currents vs. square root of the scan rate obtained from cyclic voltammetry with TMB depicted in Fig. 4 a. Experiments were performed in 500 µM TMB at pH 1 in 150 mM sodium citrate buffer with 300 mM H_2SO_4 at a screen-printed gold electrode with scan rates ranging from 0.1 – 1.2 V s^{-1}.

MALDI-TOF/MS

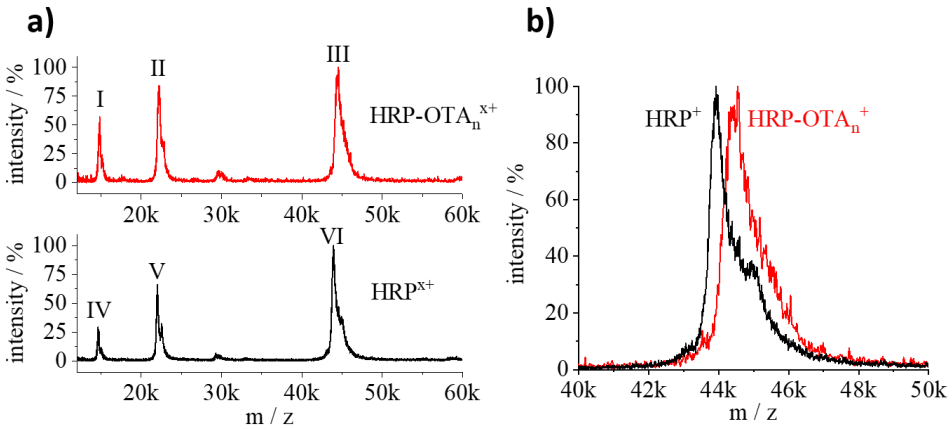

Figure S17 MALDI-TOF/MS data of the OTA-HRP Tracer and HRP as reference. **a)** shows both spectra in comparison and **b)** shows part of the spectra depicted in a), which was used for the determination of the mass. For HRP a mass of 44007 ± 42 Da (n = 6) and for OTA-HRP a mass of 44448 ± 15 Da (n = 2) was obtained.

Magnetic beads

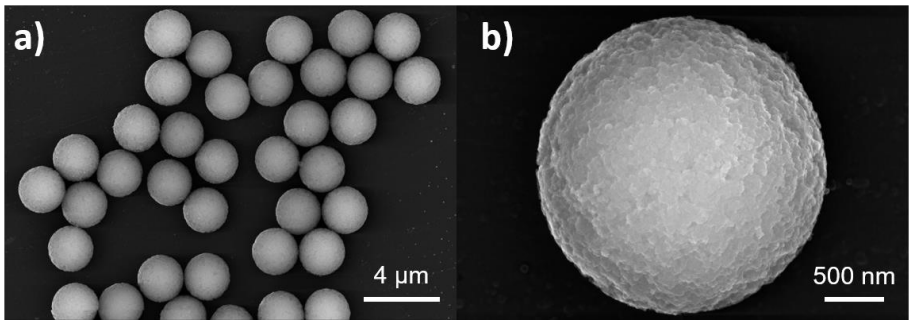

Figure S18 SEM images of protein G modified beads used for the immunomagnetic assay **a)** at low magnification and **b)** at high magnification. For both images an acceleration voltage of 20 kV was applied.

Flow cell design

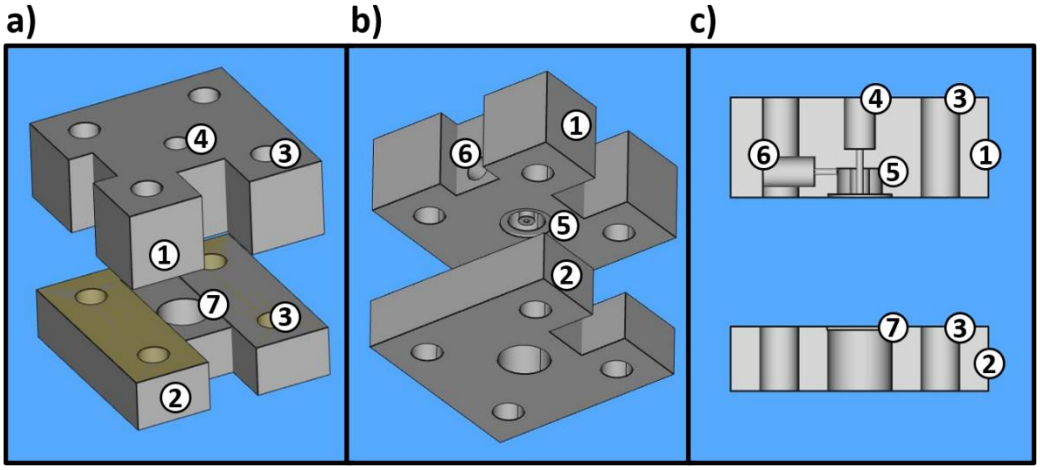

Figure S19 CAD of the custom-made flow cell for screen-printed electrodes (created with FreeCAD). **a)** Shows a top-view, **b)** a bottom-view and **c)** shows a cross-sectional view of the flow cell and the reaction chamber. The individual parts serve the following purposes: 1 – upper part of the flow cell, 2 – bottom part of the flow cell, 3 – two of eight holes for screws to press the upper and bottom part together, 4 – hole for the inlet which can be connected to a tubing system via fittings, 5 – cylindrical reaction chamber with an O-ring cavity and a smaller cylindrical nozzle connected to the inlet, 6 – hole for the outlet which can be connected to a tubing system via fittings, 7 – electrode cavity (with round hole for the optional use of a magnet).

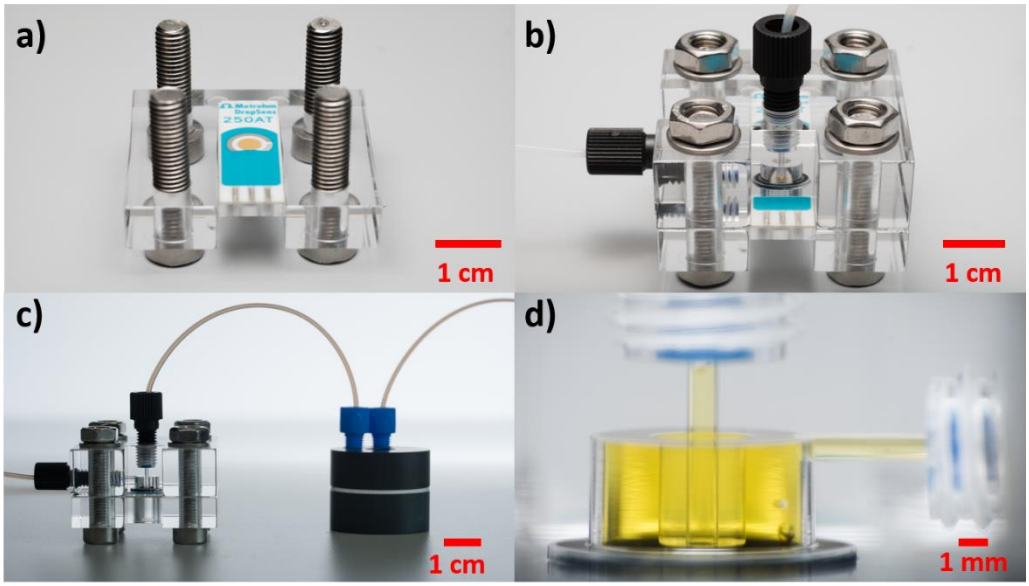

Figure S20 Photos of the custom-made flow cell for screen-printed electrodes. **a)** Bottom part of the flow cell with a screen-printed gold electrode and the screws assembled for the connection with the upper part **b)** The assembled flow cell connected via fittings to a tubing system and **c)** Flow cell with an upstream connected bubble trap and **d)** The reaction chamber with the perpendicularly arranged inlet nozzle and the horizontally arranged outlet channel (filled with solution containing fully oxidized TMB).

Amperometric measurements

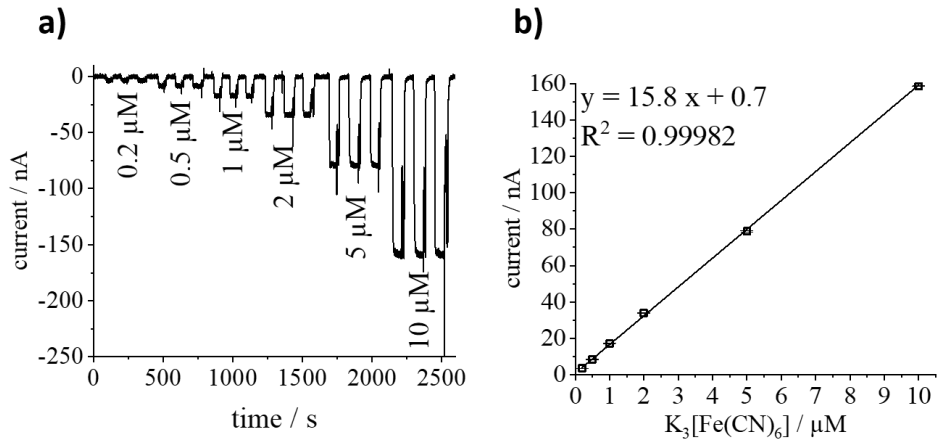

Figure S21 Testing of the custom-made flow cell by amperometric measurements with different concentrations of $K_3[Fe(CN)_6]$ in 100 mM potassium phosphate buffer with 100 mM KCl, at 0 V vs. Ag/AgCl and a flow rate of 600 µL min^{-1}. **a)** Amperometric measurement with $K_3[Fe(CN)_6]$ samples with each concentration measured three times. **b)** Redox current signal obtained from a) vs. concentration of $K_3[Fe(CN)_6]$.

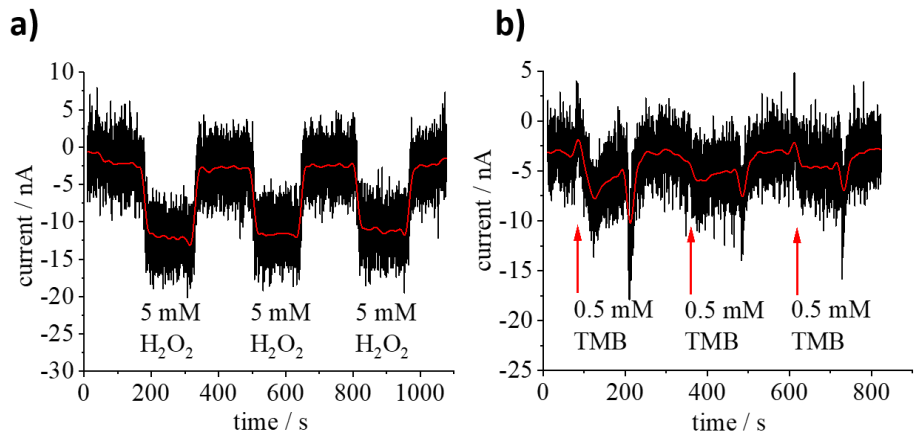

Figure S22 Amperometric measurements with **a)** 5 mM H_2O_2 and **b)** 0.5 mM TMB in 150 mM sodium citrate buffer with 300 mM H_2SO_4, 100 mM KCl with pH 1 at screen-printed gold electrodes at 300 mV vs. Ag/AgCl and a flow rate of 600 µL min^{-1}. Each sample was injected three times to study the influence of H_2O_2 and TMB in amperometric measurements. The black line shows the original signal and the red line shows the smoothed signal (100 point fast Fourier transformed).

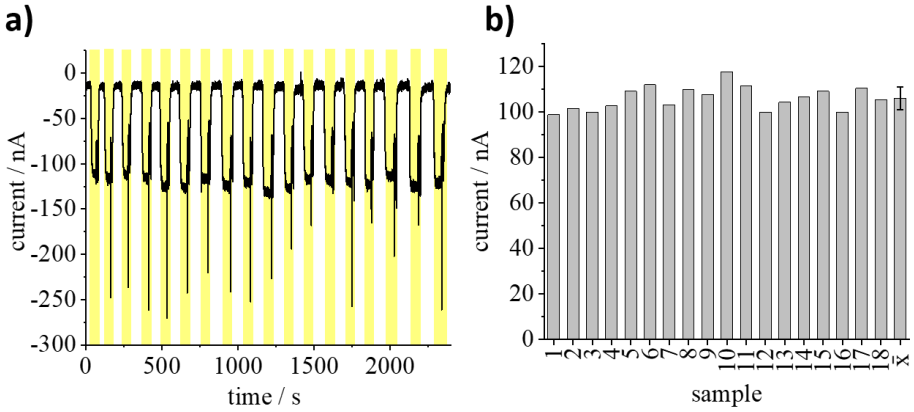

Figure S23 Repeatability of the current signal in amperometric measurements obtained for TMB in 150 mM sodium citrate buffer with 300 mM H_2SO_4, 100 mM KCl with pH 1 and screen-printed gold electrodes at 300 mV vs. Ag/AgCl and a flow rate of 600 µL min^{-1}. **a)** Amperometric measurements in which fully oxidized TMB with a concentration of 6.5 µM was injected 18 times alternately with buffer and **b)** depicts the signal intensity and its mean value of the 18 measurements.

Literature

[1] S. Rades, V.-D. Hodoroaba, T. Salge, T. Wirth, M. P. Lobera, R. H. Labrador, K. Natte, T. Behnke, T. Gross, W. E. S. Unger, *RSC Adv.* **2014**, *4*, 49577-49587.

[2] V. D. Hodoroaba, S. Rades, T. Salge, J. Mielke, E. Ortel, R. Schmidt, *14th European Workshop on Modern Developments and Applications in Microbeam Analysis (Emas 2015 Workshop)* **2016**, *109*.

[3] M. Senoner, A. Maassdorf, H. Rooch, W. Österle, M. Malcher, M. Schmidt, F. Kollmer, D. Paul, V. D. Hodoroaba, S. Rades, W. E. Unger, *Anal. Bioanal. Chem.* **2015**, *407*, 3211-3217.

[4] T. Schmid, P. Dariz, *Heritage* **2019**, *2*, 1662-1683.

[5] P. Echlin, *Handbook of Sample Preparation for Scanning Electron Microscopy and X-Ray Microanalysis*, Springer US, **2009**.
[6] M. F. Gazulla, M. Rodrigo, E. Blasco, M. Orduna, *X-Ray Spectrom.* **2013**, *42*, 394-401.
[7] a) A. Iuraş, D. J. Scurr, C. Boissier, M. L. Nicholas, C. J. Roberts, M. R. Alexander, *Anal. Chem.* **2016**, *88*, 3481-3487; b) K. De Bruycker, A. Welle, S. Hirth, S. J. Blanksby, C. Barner-Kowollik, *Nat. Rev. Chem.* **2020**, *4*, 257-268; c) A. Rohsler, O. Sobol, W. E. S. Unger, T. Bollinghaus, *Int. J. Hydrogen Energy* **2019**, *44*, 12228-12238.
[8] a) A. M. Belu, D. J. Graham, D. G. Castner, *Biomaterials* **2003**, *24*, 3635-3653; b) A. Müller, T. Heinrich, S. Tougaard, W. S. M. Werner, M. Hronek, V. Kunz, J. Radnik, J. M. Stockmann, V.-D. Hodoroaba, S. Benemann, N. Nirmalananthan-Budau, D. Geißler, K. Sparnacci, W. E. S. Unger, *J. Phys. Chem. C* **2019**, *123*, 29765-29775.
[9] a) P. Agüi-Gonzalez, S. Jähne, N. T. N. Phan, *J. Anal. At. Spectrom.* **2019**, *34*, 1355-1368; b) Q. P. Vanbellingen, N. Elie, M. J. Eller, S. Della-Negra, D. Touboul, A. Brunelle, *Rapid Commun. Mass Spectrom.* **2015**, *29*, 1187-1195; c) P. Massonnet, R. M. A. Heeren, *J. Anal. At. Spectrom.* **2019**, *34*, 2217-2228.
[10] T. Stephan, *Planet. Space Sci.* **2001**, *49*, 859-906.
[11] a) L. Van Vaeck, A. Adriaens, R. Gijbels, *Mass Spectrom. Rev.* **1999**, *18*, 1-47; b) A. Adriaens, L. Van Vaeck, F. Adams, *Mass Spectrom. Rev.* **1999**, *18*, 48-81; c) K. Schaepe, H. Jungnickel, T. Heinrich, J. Tentschert, A. Luch, W. E. S. Unger, in *Characterization of Nanoparticles* (Eds.: V.-D. Hodoroaba, W. E. S. Unger, A. G. Shard), Elsevier, **2020**, pp. 481-509.
[12] a) R. Bro, A. K. Smilde, *Anal. Methods* **2014**, *6*, 2812-2831; b) D. J. Graham, D. G. Castner, *Biointerphases* **2012**, *7*, 49; c) I. T. Jolliffe, J. Cadima, *Philosophical Transactions of the Royal Society A: Mathematical, Physical and Engineering Sciences* **2016**, *374*, 20150202; d) J. Lever, M. Krzywinski, N. Altman, *Nature Methods* **2017**, *14*, 641-642; e) J. Shiens, *Google Research* **2014**, 1-12.